Biochimica et Biophysica Acta 1798 (2010) 544–557

Contents lists available at ScienceDirect

Biochimica et Biophysica Acta

journal homepage: www.elsevier.com/locate/bbamem

The membrane insertion of helical antimicrobial peptides from the N-terminus of *Helicobacter pylori* ribosomal protein L1

Tzong-Hsien Lee [a], Kristopher N. Hall [a], Marcus J. Swann [c], Jonathan F. Popplewell [c], Sharon Unabia [a], Yoonkyung Park [b], Kyung-Soo Hahm [b], Marie-Isabel Aguilar [a,*]

[a] Department of Biochemistry and Molecular Biology, Monash University, Wellington Rd, Clayton, Vic, 3800, Australia
[b] Research Center for Proteineous Materials (RCPM), Chosun University, 375 Seosuk-Dong, Dong-Ku, Gwangju, Republic of Korea
[c] Farfield Group, Farfield House, Southmere Court, Electra Way, Crewe Business Park, Crewe CW1 6GU, UK

ARTICLE INFO

Article history:
Received 2 September 2009
Received in revised form 14 January 2010
Accepted 20 January 2010
Available online 25 January 2010

Keywords:
Antimicrobial peptide
Hp(2–20)
Surface plasmon resonance
Dual polarisation interferometry
Supported lipid bilayer
Birefringence

ABSTRACT

The interaction of two helical antimicrobial peptides, HPA3 and HPA3P with planar supported lipid membranes was quantitatively analysed using two complementary optical biosensors. The peptides are analogues of Hp(2–20) derived from the N-terminus of *Helicobacter pylori* ribosomal protein L1 (RpL1). The binding of these two peptide analogues to zwitterionic dimyristoyl-phosphatidylcholine (DMPC) and negatively charged membranes composed of DMPC/dimyristoylphosphatidylglycerol (DMPG) (4:1) was determined using surface plasmon resonance (SPR) and dual polarisation interferometry (DPI). Using SPR analysis, it was shown that the proline substitution in HPA3P resulted in much lower binding for both zwitterionic and anionic membranes than HPA3. Structural changes in the planar DMPC and DMPC/DMPG (4:1) bilayers induced by the binding of both Hp(2–20) analogues were then resolved in real-time with DPI. The overall process of peptide-induced changes in membrane structure was analysed by the real-time changes in bound peptide mass as a function of bilayer birefringence. The insertion of both HPA3 and HPA3P into the supported lipid bilayers resulted in a decrease in birefringence with increasing amounts of bound peptide which reflects a decrease in the order of the bilayer. The binding of HPA3 to each membrane was associated with a higher level of bound peptide and greater membrane lipid disordering and a faster and higher degree of insertion into the membrane than HPA3P. Furthermore, the binding of both HPA3 and HPA3P to negatively charged DMPC/DMPG bilayers also leads to a greater disruption of the lipid ordering. These results demonstrate the geometrical changes in the membrane upon peptide insertion and the extent of membrane structural changes can be obtained quantitatively. Moreover, monitoring the effect of peptides on a structurally characterised bilayer has provided further insight into the role of membrane structure changes in the molecular basis of peptide selectivity and activity and may assist in defining the mode of antimicrobial action.

1. Introduction

Recognition of the growing threat of drug resistant microbial infection as one of the world's most pressing public health problems has reinforced the urgent need for the development of new and more effective antimicrobial agents [1–3]. Short cationic amphiphilic peptides with antimicrobial and/or immunomodulatory activities are being increasingly considered as potential candidates in the development of a new generation of anti-infective therapeutic agents [4–6]. Central to these challenges is the analysis of the structure–function relationships of various antimicrobial peptides, which have established a number of specific peptide conformation/composition and activity criteria that can be incorporated into the design and synthesis of effective broad-spectrum antimicrobial peptide drugs [7,8]. In particular, these studies have helped to identify parameters that are required for optimal peptide activity [9–14]. Several critical peptide characteristics that affect antimicrobial peptide activity and specificity include the sequence/length, charge, conformation, hydrophobicity and amphipathicity of the peptides. Moreover, the composition, charge, and domain structure of lipid membranes are important in directing the selectivity toward specific microorganisms although these parameters are less well understood. While the diversity in the characteristics of antimicrobial peptides is also manifested in their diverse mechanisms of action [7,8,15–18], the precise mechanism of action is still challenging to define for a specific peptide. Importantly, the exact nature of how antimicrobial peptides selectively kill their microbial targets requires an understanding of the relative

* Corresponding author. Tel.: +61 3 9905 3723; fax: +61 3 9902 9500.
E-mail address: Mibel.Aguilar@med.monash.edu.au (M.-I. Aguilar).

0005-2736/$ – see front matter © 2010 Elsevier B.V. All rights reserved.
doi:10.1016/j.bbamem.2010.01.014

contribution of the structural characteristics of both the peptide and the membrane to the overall microbicidal mechanisms. However while the interaction between antimicrobial peptides and microbial cell membranes has been widely accepted to be a critical step in peptide action, there is very little information on the real-time dynamic changes in the membrane structure during peptide binding.

Hp(2–20) (AKKVFKRLEKLFSKIQNDK), a cecropin-like antimicrobial peptide derived from the N-terminus of *Helicobacter pylori* ribosomal protein L1 (RpL1), possesses a broad-spectrum activity against bacteria, fungi and protozoa at low micromole concentration without causing haemolysis [19–21]. In addition to their pro-inflammatory role as a monocyte chemoattractant [22,23], various analogues of Hp (2–20) have been designed and synthesised in an attempt to enhance its antimicrobial activity [24–28]. The importance of various structural characteristics of Hp(2–20), including sequence, length, conformation and amphipathicity/hydrophobicity on the antimicrobial activity has been assayed via antifungal, antibacterial and haemolytic tests [25,29] of a range of peptide analogues. One such Hp(2–20) analogue, namely HPA3 which has a double substitution of Q17W and D19W, showed 4–16 fold increased activity against bacteria and 2–4 fold higher potency at inhibiting fungal growth [24,26]. Such enhanced antimicrobial activity was attributed to the higher overall hydrophobicity and amphipathicity and longer linear helical structure as determined by CD and NMR spectroscopy in membrane-mimetic environments [25,26]. The cytolytic activity of HPA3 towards bacteria and yeast also correlated with an enhanced rate of fluorescence-dye leakage from artificial liposomes. Moreover, the correlation of the dye leakage experiments and K^+-release tests conducted on *C. albicans* demonstrated that HPA3 exerts its enhanced antimicrobial activity through peptide-induced pores with a diameter between 3.3 and 4.8 nm [26]. In addition, reproducible values of single-channel conductance of multimeric membrane-defects formed by HPA3 in zwitterionic lipid membranes at various holding potentials also support the existence of transmembrane pores [30,31]. However, in spite this extensive cytolytic data, little is known about the membrane binding characteristics of HPA3 and the role of different membrane components in the activity of the HPA3-related peptides.

Since the HPA3 peptides have been shown to form pores, they are likely to cause significant effects on the membrane bilayer structure. Thus, in order to unravel the mechanism of action, it is crucial to characterise the modulating effects on the membrane structure throughout the process of peptide binding leading to insertion. Dual polarisation interferometry (DPI) is a recently developed optical technique for real-time monitoring of thin layer deposition which can be applied to liposome adsorption, deformation and bilayer formation on a planar silicon oxynitride chip [32–36]. By simultaneously measuring the mass and thickness or density, it is possible to obtain the global structural (optogeometrical) properties of an adsorbed layer. In addition to the sub-nanometre accuracy provided by DPI, membrane birefringence [32] can also be determined to follow the process of supported lipid bilayer formation. Birefringence quantifies the degree of alignment of the lipid molecules to the planar surface and the uniaxial packing and ordering of the membrane lipids which can provide a unique insight into the process of bilayer formation and the changes in the packing and ordering of the membrane bilayer upon peptide binding [32,37–41].

In the present study, the effect of the proline substitution on the peptide structure and binding characteristics to membranes were investigated using CD and surface plasmon resonance (SPR) and DPI biosensor technology. DMPC, a neutral phospholipid was used as a model for eukaryotic cell membranes, since PC-containing phospholipids are virtually absent in bacterial membranes but are generally found as the most abundant phospholipids in fungi, yeast and mammalian cells [42]. Phosphatidylglycerols (PGs) are less abundant in eukaryotic plasma membranes but are found as the major component in bacterial membranes, particularly in Gram-positive bacteria [42]. Thus, it is also important to investigate the role of negatively charged DMPG phospholipids in mediating the structure and membrane binding-destabilisation effects of the Hp(2–20) peptide analogues. In addition, DMPC and DMPG both contain fully saturated acyl chains which allow the effect of disordering by peptides to be unaffected by the properties of unsaturated double bonds. The effect of peptide binding/insertion on the phase transition of lipid membranes was also examined. These results have provided new insight into peptide selectivity and dynamic process of insertion mechanisms in terms of changes in the geometrical structure and lipid order of the membrane bilayer and correlated the results with pore formation and the bactericidal activity of the peptide.

2. Materials and methods

2.1. Materials

1,2-dimyristoyl-sn-glycero-3-phosphocholine (DMPC), 1,2-dimyristoyl-sn-glycero-3-[phosphor-rac-(1-glycerol)] sodium salt (DMPG) were obtained from Avanti Polar Lipids (Alabaster, AL). All chemicals used were of analytical grade. 4-Morpholinepropanesulfonic acid (MOPS), sodium phosphate monobasic (NaH_2PO_4), sodium phosphate dibasic (Na_2HPO_4), sodium chloride, calcium chloride and sodium dodecylsulfonate (SDS) were purchased from Sigma-Aldrich (St. Louis, MO). Chloroform, methanol and ethanol were all HPLC grade purchased from Merck (Darmstadt, Germany). Hellmanex II was purchased from Hellma (Müllheim, Germany). Water was quartz-distilled and deionised in a Milli-Q system equipped with UV oxidation to remove organic residue (Millipore Bedford, MA, USA).

2.2. Peptide synthesis

Peptides were synthesised by solid phase methods using Fmoc-(9-florenyl-methoxycarbonyl)-chemistry. The peptides were purified using a preparative reversed phase C18 column (19×300 mm, 15 um, Deltapak C18, Waters) using an appropriate 0–60% 0.1% trifluoroacetic acid-acetonitrile gradient. Peptide purity was analysed using an analytical reversed phase C18 column (4.6×250 mm, 5 um, 300 Å, Vydac). The purified peptides were further characterised by amino acid composition analysis and matrix-assisted laser desorption ionisation (MALDI) mass spectrometer. Peptide concentration was determined by amino acid analysis.

2.3. Liposome preparation

2 mM DMPC stock in chloroform and 2 mM DMPG stock in chloroform/methanol (3:1) were used for the preparation of dried DMPC and DMPC/DMPG (molar ratio 4:1) films. The stock solutions were aliquoted out to the bottom of clean glass tubes to make the total lipid amount of 0.8 μmol. The solvent was then evaporated under a gentle stream of N_2 gas. The dried lipid films were further vacuum dried overnight to completely remove the residual organic solvent. The dried lipid thin films were hydrated with a running buffer, 10 mM MOPS, pH 7.0, 150 mM NaCl to make a lipid concentration of 1 mM. Hydration was kept at 37 °C for 1.5 h with constant vortexing. The hydrated lipid suspension was then sonicated in a 37 °C water bath for 30 min. The clear liposome solution was then extruded through a 50 nm polycarbonate membrane 21 times using an AVESTIN Liposofast extruder (Avestin, ON, Canada). The size distribution of resulting small unilamellar vesicles (SUVs) was characterised by dynamic light scattering with a Malvern Zetasizer 3000 using a 5 mW HeNe laser and the Windows PCS version 1.31 software (Malvern Laboratories Ltd., Malvern, UK).

2.4. Circular dichroism (CD) analysis

CD experiments were performed using a Jasco 815 spectropolarimeter (Jasco, MD, USA) using a 0.1 cm path length quartz cell. All spectra were obtained at 20 °C. DMPC and DMPC/DMPG (4:1) small unilamellar vesicles prepared by hydrating in 10 mM sodium phosphate buffer, pH 7.4 and were extruded through a polycarbonate filter (100 nm pore diameter). The peptide (1 mM in sodium phosphate buffer) was then added to the liposome solution at a final peptide concentration of 20 μM resulting in a peptide:lipid molar ratio of 1:50. The peptide–liposome solution was mixed by inversion and incubated for 2 min. Each spectrum was obtained by averaging five scans in the 190–260 nm wavelength range. All CD spectra are reported in mean residue ellipticity $[\theta]$ in deg cm^2 $dmol^{-1}$. The α-helical content was calculated from the mean residue ellipticities at 222 nm ($[\theta]_{222}$) according to

$$\%[\alpha] = \frac{[\theta]_{222}}{[[\theta]_{\text{helix}} \cdot (1-2.57/n)]} \times 100 \quad (1)$$

where $[\theta]_{\text{helix}}$ is the ellipticity of a peptide of infinite length with 100% helix with a value of −39,500 deg cm^2 $dmol^{-1}$, and n is the number of residues in each peptide.

2.5. Surface plasmon resonance (SPR)

SPR experiments were carried out with a Biacore T100 analytical system with an L1 sensor chip (Biacore, Uppsala, Sweden). The system was cleaned using the standard Desorb and Sanitize protocol with a maintenance chip and then allowed to run overnight with water. The L1 chip was docked and first washed with an injection of 5 μL of 20 mM CHAPS at a flow rate of 5 μL/min to clean the chip surface. Prior to the liposome immobilisation, the temperature was adjusted to 20 °C. SUVs in immobilisation buffer (10 mM MOPS pH 7.0, 150 mM) were injected at a flow rate of 2 μL/min for 40 min. At the end of liposome injection, 30 μL of 10 mM NaOH was injected at 50 μL/min. All solutions were freshly prepared, degassed and filtered through a 0.22 μm nylon membrane filter. In our experiments lipid deposition led to deposition levels above 5000 RU for all lipid mixtures which suggests that the lipid surface has a similar bilayer structure in each case indicating an optimum surface coverage.

The peptide solutions were prepared by dissolving HPA3 and HPA3P in the running buffer for a 100 μM peptide stock. Peptide solutions at eight concentrations ranging from 0.1 μM to 20 μM were prepared from the peptide stock 1 mM. 100 μL of each peptide solution was injected at a flow rate of 30 mL/min having a total injection of 200 s. On completion of injection, buffer flow continued to allow a dissociation time of at least 600 s. All binding experiments were carried out at 20 °C. The affinity of the HPA3 and HPA3P to the membrane binding event was determined from a series of response curves for each set of peptide−membrane combinations.

2.6. Kinetic and affinity constant calculation

The sensorgrams for each peptide−membrane interaction were analysed by numerical integration curve-fitting algorithm [43,44]. The BIAevaluation 3.0 software (Biacore, GE Health) provides different reaction models to perform complete kinetic analysis of the peptide−membrane interaction. On the basis of the possible binding mechanisms of Hp(2−20) peptides to the membrane, a two-state reaction model was chosen for the estimates for kinetic constants including the association (k_a) and dissociation (k_d) rate constants and affinity constants [43,45]. The resultant sensorgrams of each peptide were fit locally to the RU_{max} obtained at 0.1−20 μM.

2.7. Dual polarisation interferometry

Dual polarisation interferometry (DPI) is an analytical method for analysing thin films using a dual optical waveguide interferometric technique. Alternate dual orthogonal polarisation allows unique combinations of several optogeometrical properties including refractive index (RI), density, thickness, mass and birefringence to be measured in real-time for the formation of biomolecule layers.

DPI, as deployed in the *Ana*light BIO200 (Farfield Group Ltd., Manchester, UK), consists of a dual slab waveguide sensor chip with an upper sensing waveguide and a lower optical reference waveguide illuminated with an alternating polarised laser beam (HeNe, wavelength 632.8 nm). As shown schematically in Fig. 1A, the sensor chip comprises four layers of deposited silicon oxynitride on a silicon wafer surface. Two orthogonal polarizations are passed through the sensor chip creating two different waveguide modes, namely transverse electric (TE) and transverse magnetic (TM) waveguide modes. Each TM and TE mode generates an evanescent field from the top sensing waveguide surface interacting with materials coming into contact with the sensor surface and resulting in a change in refractive index. When this occurs the phase difference between the sensing waveguide and the buried reference waveguide is altered and the position of the interference fringes changes. In this way the sensor is capable of measuring very subtle molecular changes that occur on the sensor surface. The interference fringe pattern for each TM and TE waveguide mode shown as the diffraction fringe image, illuminates a 1024×1024 element-imaging device in the far-field, the output of which is passed to the digital signal processing unit. The relative phase position is updated every 2 ms using a spatial Fourier transform method. Two separate measurements of fringe shift TM and TE data are transferred to a personal computer for further analysis to provide a real-time data display and to further resolve the data into thickness and refractive index values for the growing layer.

Unmodified silicon oxynitride FB80 AnaChips (Farfield Group, UK) were used for the preparation of a supported lipid bilayer (SLB). The sensor chip (dimensions 24×6 mm) is clamped inside a dual-zone temperature-controlled housing capable of controlling chip temperature by a Peltier system to within ±0.005 °C. A 100 μm thick fluorosilicon mask with two slots is clamped on top of the waveguide chip which provides two separate microfluidic channels over the sensing waveguide. Each flow channel has a dimension of 1 mm wide and 17 mm long which forms a 1.7 μL measurement chamber.

These chips were cleaned on-line by rinsing 3 times with 10% Hellmanex II followed by 3 times with 2% SDS and finally rinsing 3 times with absolute ethanol. Prior to measurement, the waveguide chips were calibrated with respect to their optical properties using an 80:20 w/w ethanol/water mixture at 20 °C. All experiments were conducted in 10 mM MOPS pH 7.0, 150 mM NaCl. The flow rate of the running buffer was controlled using a Harvard Apparatus PHD2000 programmable syringe pump. Typical flow rates were 20 μL/min for liposome deposition and 40 μL/min for peptide binding to the SLB. *Ana*Light200 version 2.1.0 software was used for data acquisition and the acquired data were analysed using *Ana*Light® Explorer proprietary software. Data were acquired at 10 Hz and averaged to give an output of one data point per second.

2.7.1. Supported lipid bilayer formation

Liposome solutions (0.1 mg/mL) of DMPC and DMPC/DMPG (4:1) were injected in the presence of 1 mM $CaCl_2$ for 10 min at 20 μL/min at 28 °C. The adsorption was immediately followed by injecting 1 mM $CaCl_2$ in the running buffer for 10 min which facilitates the stabilisation of the SLB on the solid substrate. The SLB was further equilibrated in the running buffer without Ca^{2+} for 20 min before adjusting the temperature to 20 °C. The

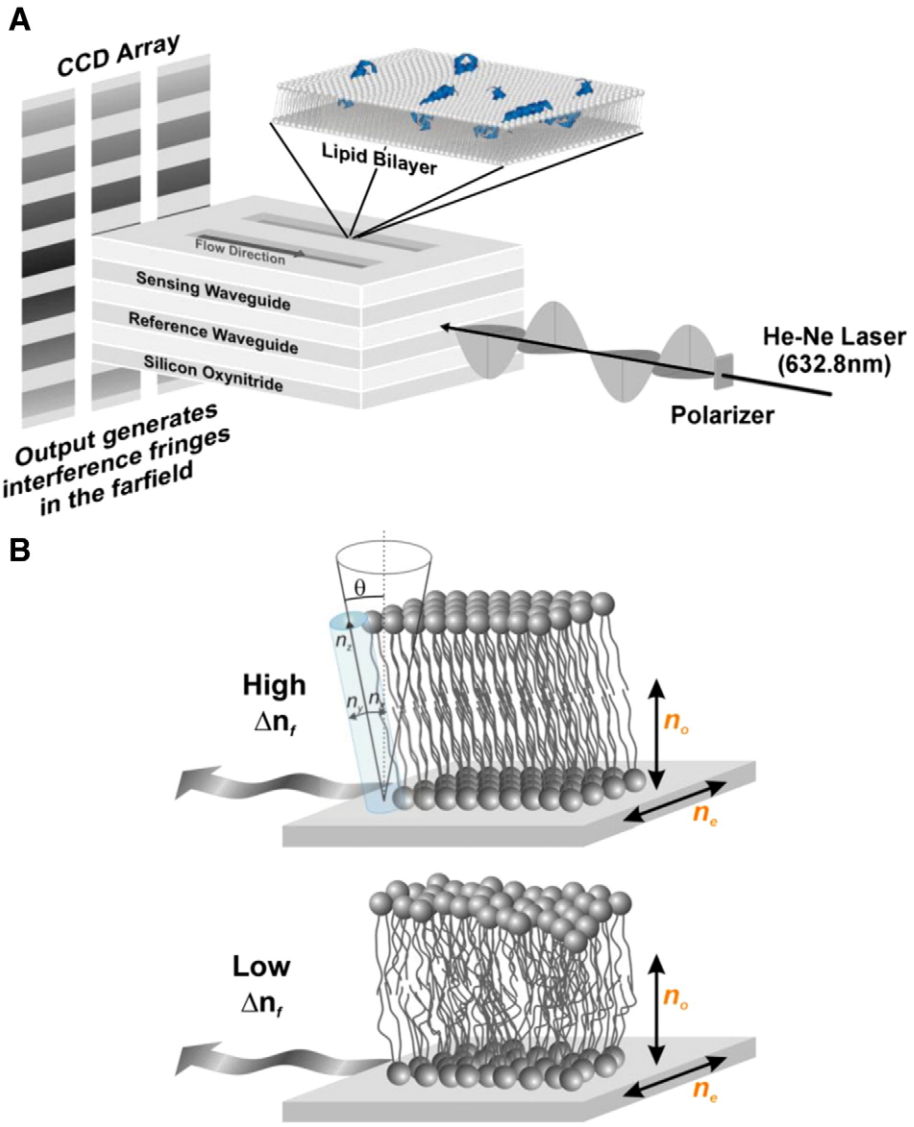

Fig. 1. (A) Biomembrane chip with dual polarisation interferometer (DPI) consists of a dual slab waveguide guiding light through two high-refractive index structure (sensing waveguide and reference waveguide). Two orthogonal polarisations, TM and TE, pass through the waveguide forming two evanescent fields which are affected by the molecules binding onto the surface. Such changes for each TM and TE are detected separately as a phase shift in the fringe pattern at the far-field. Thus, the formation of a unilamellar planar bilayer via liposome adsorption and the dynamic impact of peptide binding on the lipid bilayer structure can be quantitatively analysed in real-time. (B) The optical birefringence (Δn_f) of a fully aligned/ordered (top) and a disordered (bottom) unilamellar supported lipid bilayer. The molecular refractive index (RI) in x (n_x) and y (n_y) horizontal dimensions is different from RI in the z vertical dimension (n_z). Birefringence is a measure of the difference between RI parallel with surface (n_e) and RI perpendicular to surface (n_o). Thus, the changes in the packing, alignment and degree of order of lipid molecules assembled on the surface can be determined from quantitatively analysing changes in birefringence.

coverage and quality of membrane was checked with 50 µL injection of 50 µg/mL BSA. A full lipid bilayer-covered silicon oxynitride chip was confirmed by the absence of BSA binding to the membrane bilayer.

2.7.2. Peptide injection

HPA3 and HPA3P were prepared at concentrations of 5 µM, 10 µM, and 20 µM in 10 mM MOPS, pH 7, 150 mM NaCl. Peptide samples were injected consecutively in order of increasing concentration onto the deposited bilayer at 20 °C. 180 µL of each peptide concentration was injected at a flow rate of 40 µL/min, followed by running buffer for 30 min prior to injecting the next concentration onto the same bilayer surface. Each peptide concentration measurement was performed on the same lipid bilayer, after which the waveguide surface was regenerated with 2% SDS, 10% Hellmanex II and ethanol at 28 °C.

2.7.3. Optical birefringence analysis for the dynamic changes in membrane lipid order

Birefringence (optical anisotropy) is a measure of the difference in refractive index of two orthogonal polarisations [37,40,41]. Among various types of thin films, phospholipid bilayers show optical birefringence owing to the liquid crystal properties of lipid molecules self-assembled into uniaxial aligned bilayers. As shown in Fig. 1B, top, the non-random orientation of lipid molecules in a membrane creates an anisotropic system with a uniaxial optical axis with two principal refractive indices, namely, the extraordinary refractive index ($\boldsymbol{n}_e$) which denotes the electric vector polarised parallel to the optical axis, and the ordinary refractive index ($\boldsymbol{n}_o$) which denotes the electric vector polarised perpendicular to the optical axis. The difference between these two refractive indices for a lipid film is defined as the birefringence Δn_f as the following,

$$\Delta n_f = \boldsymbol{n}_e - \boldsymbol{n}_o. \quad (2)$$

Thus, birefringence can be obtained with dual polarisation interoferometry through calculating the difference between the two effective refractive indices, namely refractive index of transverse magnetic (TM) waveguide mode (n_{TM}) and refractive index of transverse electric (TE) waveguide mode (n_{TE}). The degree of molecular order, S, of the uniaxial lipid bilayer is defined by the ratio of the principal polarizabilities of the bilayer to the molecular polarizabilities [40]. This order parameter (S) is proportional to the birefringence values. Thus, the birefringence values represent an averaged measurement of lipid molecular orientation order and the lipid acyl chain order. As shown in Fig. 1B, high Δn_f values are obtained for a fully aligned lipid bilayer whereas low Δn_f indicates a randomly ordered lipid bilayer.

The effective birefringence ($n_{TM} - n_{TE}$) can only be determined by calculating the two different refractive indices, n_{TM} and n_{TE} for each waveguide mode by fixing the thickness or RI of the deposited layer and assuming a uniform layer coverage. The n_{TM} is affected by the layer thickness and both n_e and n_o as follows,

$$n_{TM} = \sqrt{n_e^2 \sin^2\theta + n_o^2 \cos^2\theta} \quad (3)$$

where θ, the mode angle denotes the angle between the optical axis of the adlayer and the mean path of the two wave mode as shown in Fig. 1B, top, while the n_{TE} is affected only by the layer thickness and n_o as

$$n_{TE} = n_o \quad (4)$$

According to Eqs. (3) and (4), both n_e and n_o can be calculated from n_{TM} and n_{TE}.

The respective effective adlayer n_{TM} and n_{TE} corresponding to the measured TM and TE phase changes are calculated by fitting the data to a waveguide equation [32]. When a correct thickness is used for an anisotropic layer, the difference between the n_{TM} and n_{TE} will be the true effective birefringence of the adlayer [46]. For deposition of a lipid bilayer, a constant thickness is assumed for the entire process [32], corresponding to the steric thickness obtained by neutron scattering and X-ray reflectivity. For the purposes of the present study, an assumed thickness for both the DMPC and DMPC/DMPG layer was fixed at the 4.6 nm for the supported lipid bilayer formation at 20 °C [47,48]. When the thickness is fixed for an anisotropic lipid bilayer, changes in refractive index (RI) and therefore density and mass can be further calculated for the supported lipid bilayer. Similarly, changes in the thickness of the deposited bilayer can also be resolved by fixing the refractive index at a predetermined value of 1.47 for DMPC and DMPG.

2.7.4. Calculation of mass for an anisotropic layer

To calculate the mass of an adsorbed molecular layer from DPI measurements, de Feijter formula was employed. The mass of lipid bilayer (m_{lipid}) formed on the solid support is calculated as follows:

$$m_{lipid} = d(n_{iso} - n_{buffer}) / (dn/dc)_{lipid} \quad (5)$$

and the mass of peptides ($m_{peptide}$) bound to the lipid bilayer is calculated as follows:

$$m_{peptide} = d(n_{iso} - n_{buffer}) / (dn/dc)_{peptide} \quad (6)$$

where n_{iso} denotes the average or corresponding isotropic refractive index of the adlayer and is calculated according to

$$n_{iso} = \sqrt{(n_{TM}^2 + 2n_{TE}^2)/3} \quad (7)$$

and n_{buffer} is the refractive index of the MOPS buffer used for these experiments which was obtained experimentally as $n_{buffer} = 1.3349$ ($T = 20$ °C). The dn/dc is the specific refractive index increment of the adlyer. The de Feijter formula assumes that dn/dc remains constant throughout the whole process of the experiment. For the present analysis, the dn/dc values of 0.135 mL/g and 0.182 mL/g were used for lipids and peptides, respectively [32].

3. Results

3.1. Peptide secondary structure determined by circular dichroism (CD)

The effect of proline substitution on the secondary structure of HPA3 in aqueous buffer and lipid media was examined with CD and the resulting spectra for HPA3 and HPA3P shown in Fig. 2A and B respectively. In 10 mM sodium phosphate buffer (pH 7.4), 20 μM HPA3 and HPA3P (sequences listed in Table 1) showed CD spectra with a single minimum at about 198 nm which is characteristic for an extended structure (grey line). In the presence of DMPC liposomes, the spectrum showed a single maximum at 190–195 nm and a double minimum at 205 and around 220 nm which indicated the formation of α-helical conformation. This corresponded to a calculated % helix of 11.1% for HPA3 (Fig. 3A, red line) while negligible secondary structure was observed for HPA3P with 2.4% helix in DMPC media (Fig. 3B, red line). However, in the presence of DMPC/DMPG (4:1) liposomes, both HPA3 and HPA3P adopted helical structure. The percentage of helicity obtained for HPA3 in DMPC/DMPG was 26.2% which is higher than the helix content obtained for HPA3P (14.3%) in the same lipid media. Overall, these results show that the proline substitution at the middle of HPA3 peptide caused a marked reduction in helix formation in a membrane environment.

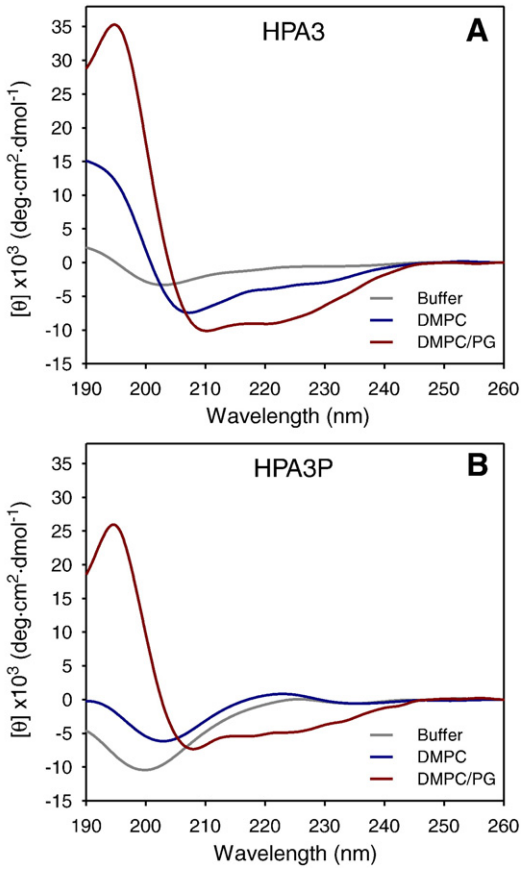

Fig. 2. CD spectra of (A) 20 μM HPA3 and (B) HPA3P in 10 mM sodium phosphate buffer, pH 7.4 (grey line), 1 mM DMPC (blue line) and 1 mM DMPC/DMPG (4:1) liposomes (red line).

Table 1
The molecular weight, net charge and sequences of antimicrobial peptides binding to planar solid-supported membranes.

No.	Peptides	M.W.	Charge	Sequence																	
1	HPA3	2448.20	+6	A	K	K	V	F	K	R	L	**E**	K	L	F	S	K	I	W	N	W	K
2	HPA3P	2417.20	+7	A	K	K	V	F	K	R	L	**P**	K	L	F	S	K	I	W	N	W	K

3.2. SPR measurement of Hp(2–20) analogue binding to lipid membranes

The binding of HPA3 and HPA3P to zwitterionic DMPC and anionic DMPC/DMPG (4:1) bilayers was measured in real-time by SPR and sensorgrams obtained at eight different peptides concentrations between 0.1 and 20 μM are shown in Fig. 3. The dependence of the RU on the peptide concentration at the end of the injection at 200 s indicates that the amount of peptide bound to lipids is approximately proportional to the injected peptide concentration between 2.5 and 20 μM. However, no significant change in response was observed for these peptides at lower concentrations between 0.1 and 0.5 μM. Thus, a minimum peptide concentration of 0.5 μM was required for the interaction and effects on the membrane to be analysed.

HPA3 readily adsorbed onto the DMPC bilayer, giving very high RU values with a RU_{max} of 4780 RU at 20 μM. These values were significantly higher than the RU values observed for the binding of HPA3P to DMPC (RU_{max} of 1250 RU at 20 μM HPA3P). The role of negatively charged lipids in peptide binding was also analysed. Again, a higher response was observed for HPA3 than for HPA3P on DMPC/DMPG. However, there was little difference between the RU_{max} for each peptide bound to zwitterionic DMPC compared to anionic DMPC/DMPG membranes demonstrating that the potential increase in electrostatic interactions with the additional 20% anionic DMPG did not occur. Overall, the binding of HPA3 to both DMPC and DMPC/DMPG exhibited a 4-fold increase in RU_{max} relative to HPA3P. The higher RU_{max} of HPA3 obtained for both DMPC and DMPC/DMPG can be correlated with a greater exposure of the hydrophobic surface as reflected by the longer retention time of HPA3 when analysed by C18 RP-HPLC (3.6 min later than HPA3P on a 0–50% acetonitrile gradient over 30 min). Thus, the proline substitution not only lowered the overall hydrophobicity but also reduced membrane binding.

As the binding did not reach equilibrium during the association phase, the affinity constants could not be calculated from the dependence of RU_{max} and peptide concentrations by fitting the data to a steady-state affinity model [43,45]. Curve-fitting of sensorgrams to a two-state reaction model was thus performed in order to obtain quantitative information on the affinity and the kinetic rate constant of the binding. However, high χ^2 values (i.e. >700) were obtained indicating significant deviation from the two-state model of peptide–membrane interaction.

3.3. DPI measurement of Hp(2–20) analogues binding to lipid membranes

3.3.1. Characterisation of the deposited lipid bilayer

The formation of a homogeneous, defect-free and fully aligned supported lipid bilayer is crucial in acquiring accurate quantitative

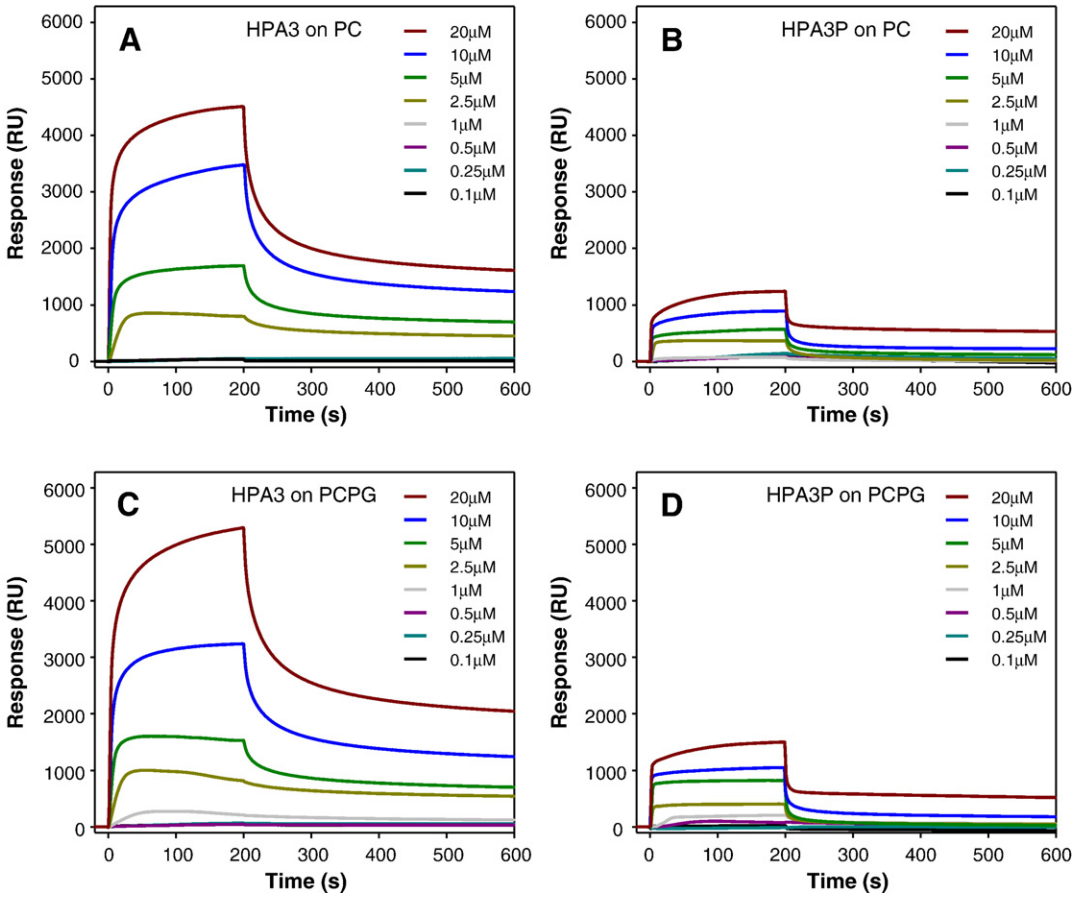

Fig. 3. SPR sensorgrams of Hp(2–20) analogues binding to DMPC and DMPC/DMPG (4:1) membranes. Peptides were injected at a concentration ranging from 0.1 to 20 μM. (A) HPA3 to DMPC, (B) HPA3P to DMPC, (C) HPA3 to DMPC/DMPG and (D) HPA3P to DMPC/DMPG.

Table 2
Structural parameters of a unilamellar phospholipid bilayer formed via direct adsorption of small unilamellar vesicles (50 nm SUVs) onto a planar silicon oxynitride.

Lipid	RI[a]	Density[a] (g/cm^3)	Thickness[b] (Å)	Mass (ng/mm^2)	Birefringence	Area (Å^2/lipid)
DMPC ($n=8$)	1.4663 ± 0.0019	0.97 ± 0.01	44.7 ± 0.7	4.48 ± 0.06	0.0215 ± 0.0007	50.29 ± 0.73
DMPC/DMPG (4:1) ($n=8$)	1.4747 ± 0.0046	1.04 ± 0.04	47.6 ± 1.6	4.77 ± 0.16	0.0235 ± 0.0015	47.44 ± 1.59

[a] The isotropic refractive index and density were calculated using the fixed thickness of 4.6 nm for DMPC and DMPC/DMPG at 20 °C as determined by neutron scattering [47,50].
[b] The thickness is calculated using the fixed isotropic refractive index of the lipid film of 1.47 [32].

information on changes in the membrane structure induced by the Hp (2–20) peptide analogues. The structural characteristics obtained for the planar DMPC and DMPC/DMPG bilayers formed via liposome adsorption onto the planar silicon oxynitride are listed in Table 2. The average values of the planar bilayer thickness obtained for DMPC and DMPC/DMPG were 44.7 Å and 47.6 Å, respectively. Based on the deposited mass per unit surface area, the surface area per lipid molecule was also calculated for each membrane bilayer, and found to be 50.3 Å^2 and 47.4 Å^2 for DMPC and DMPC/DMPG bilayer respectively. These values correlate closely with the reported values obtained from X-ray reflectivity and neutron reflectivity studies [47–50]. The structures for both membrane compositions were also highly reproducible for all supported lipid bilayers formed at 20 °C, with the standard deviations between lipid deposition being 1.2% and 3.3% for DMPC and DMPC/DMPG, respectively. These consistent and homogenous membrane structures were then used for investigation of the real-time binding of each peptide.

3.3.2. Binding of Hp(2–20) analogues to planar supported lipid bilayers

The dynamics of structural changes occurring within the aligned unilamellar phospholipid bilayer upon the binding of HPA3 and HPA3P were then examined with simultaneous real-time measurement of changes in TM/TE, mass and birefringence. For each binding experiment, peptides were injected at 5, 10 and 20 μM accumulatively onto the same lipid bilayer. This concentration range was selected from the upper concentrations which exhibited a linear dependence of the RU on peptide concentration in the SPR experiments. It should be noted that consecutive accumulative injections were performed. That is, the 5 μM injection was made on a fresh membrane, while the 10 μM sample was injected onto the same surface which contained residually bound peptide from the 5 μM injection. Similarly, the 20 μM sample was injected onto the same surface following the 10 μM injection. This experimental design was used to explore the effects of accumulative exposure of the bilayer surface to each peptide. The real-time TM and TE phase changes for HPA3 and HPA3P binding to DMPC and DMPC/DMPG are shown in Fig. 4 and show significant differences between each peptide and each bilayer. In order to relate these changes to more specific molecular parameters, the TM/TE values were then used to calculate the corresponding real-time mass changes and are shown in Fig. 5. There was a rapid increase in the mass upon injection of both HPA3 (Fig. 5A and B) and HPA3P (Fig. 5C and D) to both planar bilayers at 5 μM. However, for subsequent

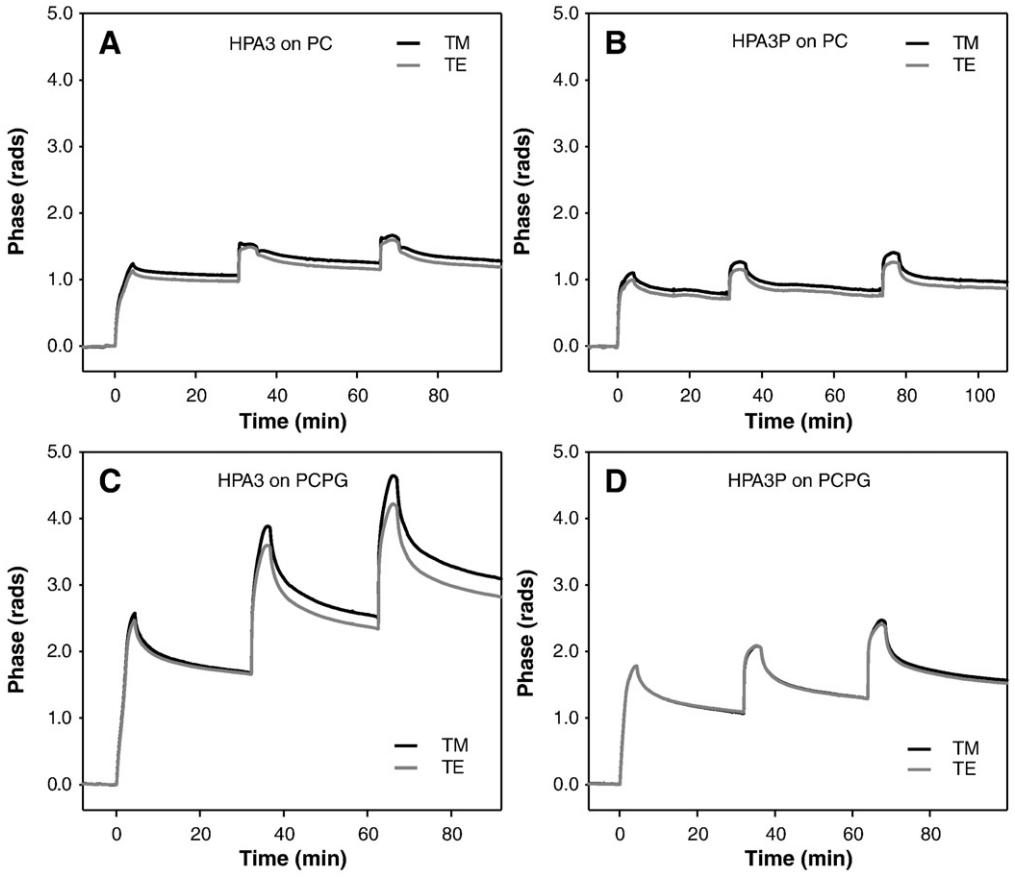

Fig. 4. Real-time TM and TE phase changes for the consecutive injection of 5, 10 and 20 μM peptide solution to a planar supported DMPC and DMPC/DMPG (4:1) bilayer. (A) HPA3 to DMPC, (B) HPA3P to DMPC, (C) HPA3 to DMPC/DMPG and (D) HPA3P to DMPC/DMPG.

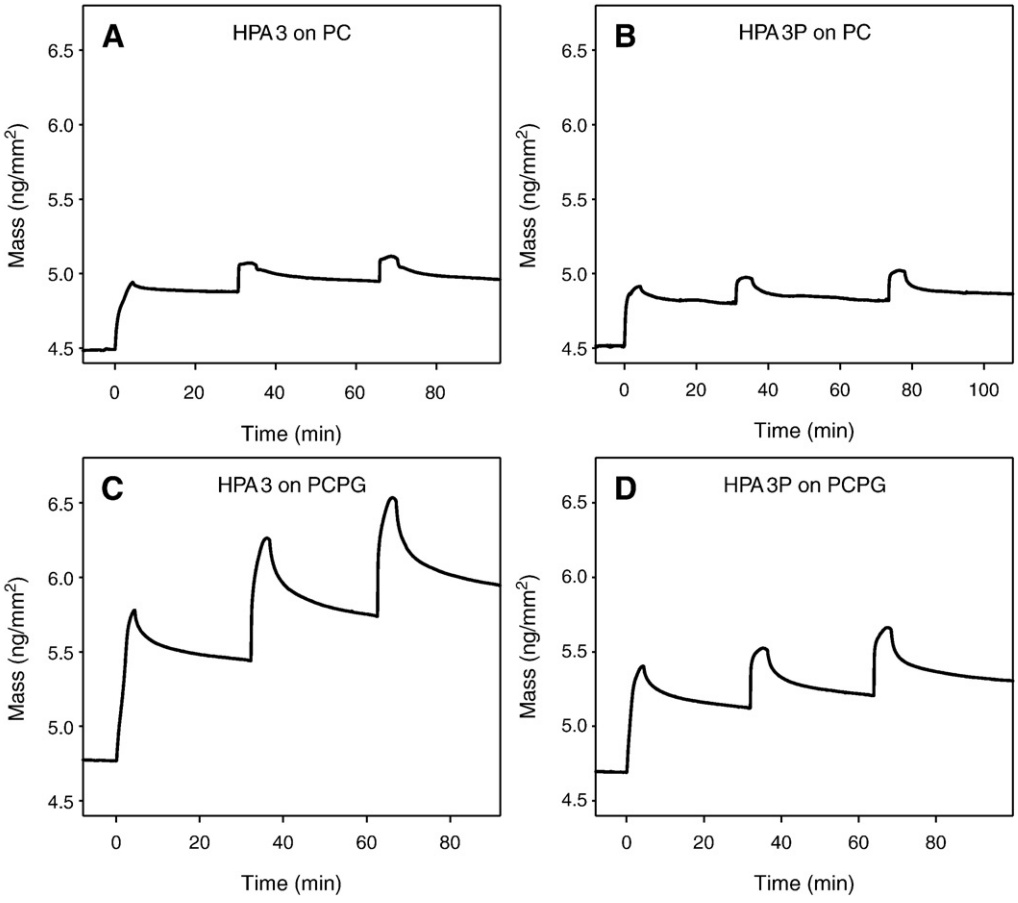

Fig. 5. Real-time mass changes for the consecutive injection of 5, 10 and 20 μM peptide solution to a planar supported DMPC and DMPC/DMPG (4:1) bilayer. (A) HPA3 to DMPC, (B) HPA3P to DMPC, (C) HPA3 to DMPC/DMPG and (D) HPA3P to DMPC/DMPG.

injections at 10 and 20 μM, the magnitude of the increase in TM/TE and mass was not proportional to the peptide concentration, as the degree of change became smaller and smaller with the increase from 10 to 20 μM peptide. These results indicate that the accumulated peptide injection did not result in further proportional increases in the amount of peptide bound to the membrane. If the dissociation phase is then analysed, there was a small decrease in mass at the end of injection for both peptides at 5 μM which indicates a strong retention of the peptides within the membrane at this low concentration. At the higher concentrations, there was a smaller increase in the residually bound peptide as a higher proportion of the adsorbed peptide dissociated at the end of the injection. This significant level of residually bound peptide may be a consequence of irreversible insertion of peptides into the bilayer [51] and is qualitatively consistent with the SPR data.

3.3.3. Effect of Hp(2–20) analogues on membrane lipid ordering as indicated by birefringence

The changes in the value of mass and birefringence for both the DMPC and DMPC/DMPG bilayers at the end of each peptide injection at 5, 10, and 20 μM are plotted in Fig. 6. Fig. 6A summarises the end-of-injection data derived from Fig. 5 and shows HPA3 bound to a greater extent on both lipids than HPA3P in which the mass was 1.4 fold higher and 1.8 fold higher for HPA3 than HPA3P with DMPC and DMPC/DMPG, respectively. In addition, the data shows that both peptides bound more on the DMPC/DMPG mixed bilayers than the DMPC bilayer. While this appears a larger difference when compared to the SPR data shown in Fig. 4, each peptide injection was made on a fresh membrane surface in the SPR experiments, in contrast to the accumulative injection protocol used in the DPI experiments. It is interesting to note that the difference in the SPR response for each peptide on different bilayers is less than the mass changes observed in the DPI analysis. The structure of the bilayer on the DPI chip is very precisely determined — while the liposome structure on the SPR chip may be comprised of unruptured liposomes together with some multilayer bilayers. It is possible that these differences lead to differences in the amount of peptide that can bind per/unit area of bilayer surface.

Birefringence is a quantitative measure of the membrane order [32,38,40,41] and birefringence values were determined as described in the Materials and methods. A decrease in the birefringence correlates with a decrease in the order or an increase in the disorder of the membrane packing and is therefore a sensitive probe of the overall integrity of the membrane structure. HPA3 induced greater changes in membrane structure than HPA3P on both supported bilayers, as shown in Fig. 6B, where more pronounced decreases in birefringence were observed for HPA3 than HPA3P binding to both lipid bilayers. In addition, the binding of HPA3 and HPA3P to the anionic DMPC/DMPG bilayer caused much larger decreases in birefringence than for DMPC as evident by 2.0 fold and 2.4 fold decreases in DMPC/DMPG birefringence for HPA3 and HPA3P respectively. This result indicates that the DMPC/DMPG bilayer, which is initially more tightly packed, becomes more disordered than the DMPC bilayer as a result of initial peptide binding at 5 μM. However, subsequent accumulated addition of peptide to the bilayer did not result in significant further decreases in the birefringence and mass. Overall, these mass and birefringence results suggest that HPA3P induces a greater disordering of the DMPC/DMPG bilayer per unit peptide mass than HPA3, most likely due to the presence of the proline residue that causes a bend in the helical structure which in turn disrupts the aligned lipid bilayer.

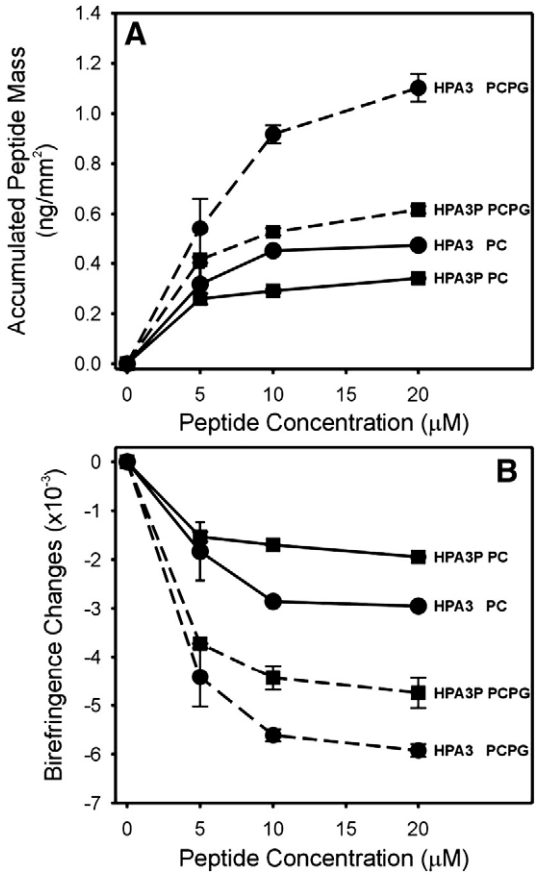

Fig. 6. Hp(2–20) analogues, HPA3 (circle) and HPA3P (square), induced changes in the (A) mass and (B) birefringence of planar supported DMPC (solid line) and DMPC/DMPG (4:1) (dash line) bilayer for 5, 10, and 20 μM peptide concentration.

The change in lipid molecule ordering as a function of bound peptide mass can be further examined by the plot of bilayer birefringence versus peptide mass as shown in Fig. 7. The binding of these peptides to both supported lipid bilayers resulted in decreases in birefringence at each concentration indicating a significant disordering in the lipid molecules induced by the peptides. If the data for HPA3 on DMPC is considered first, it can be seen that at 5 μM, there is a linear decrease in birefringence with increasing mass. However, the birefringence and mass values do not return to the initial values at the end of the injection indicating residually bound peptide and permanent change to the membrane order. Upon the 10 μM and 20 μM injections, there is a further linear decrease in birefringence, with the mass and birefringence values returning to the post 5 μM values by the end of each injection. Such reversible changes in birefringence indicated that the further addition of peptide only resulted in transient changes in the lipid ordering and that the bilayer can re-align after the peptide dissociates from the bilayer. Similar birefringence-mass profiles were observed for HPA3P on DMPC, but smaller changes in birefringence were evident reflecting a smaller perturbation of DMPC membrane structure by HPA3P.

The overall magnitude of decreases in birefringence at 5 μM was significantly larger for both peptides on DMPC/DMPG. Regression analysis of the association of HPA3 and HPA3P was performed at 5 μM — the extent of birefringence changes as a function of peptide mass was greater for their binding to DMPC/DMPG (−0.0075/ng/mm^2) than to DMPC (−0.0061/ng/mm^2). These results reflect a greater disruption of lipid packing to the DMPC/DMPG bilayer most likely as a result of insertion into the membrane.

3.3.4. The thermal phase transition of Hp(2–20) analogue-bound membranes

The changes in birefringence as a function of temperature also provide a sensitive tool to examine the impact of the HPA3 peptides on the phase transition behaviour of the adsorbed DMPC and DMPC/DMPG. As shown in Fig. 8, a distinctive phase transition (Tm) was observed at 21.8 °C and 23.7 °C for pure DMPC and mixed DMPC/DMPG bilayers respectively. Moreover, changes between the ordered and disordered state of DMPC as determined by birefringence are directly analogous to the phase transition between gel and liquid-crystalline states determined by the excess heat capacity using DSC. The data shown in Fig. 8 are thermal denaturation curves thereby demonstrating the effects of the phase transition on the binding characteristics of the peptide while the lipids undergo a change in structure. Specifically, the birefringence values were 0.0215 for gel-phase DMPC and 0.0235 for gel-phase DMPC/DMPG. In comparison, the birefringence values were 0.0185 for liquid-crystalline DMPC and 0.0221 for liquid-crystalline DMPC/DMPG. The increase in Tm from 21.8 °C to 23.7 °C in the presence of the anionic lipid is consistent with the phase behaviour examined by DSC [52,53] and reflects a higher ordering for DMPC/DMPG which is also evident from a higher birefringence value (Table 2).

This data can then be compared to the effect of bound peptide on the shape of the transition and the value of the transition temperature. For DMPC, the birefringence dropped from 0.0215 to 0.02 upon binding of each peptide. During heating, this value remained constant (Fig. 8A) up to 22 °C and was then followed by a distinct phase transition obtained at 24.5 °C. As the temperature increased further, the subsequent decrease in birefringence was greater for the HPA3P–DMPC complex (final value = 0.0176) than for HPA3–DMPC (final value = 0.0183). In other words, HPA3P induced a greater degree of change in thermal induced birefringence than HPA3. Thus, the HPA3-bound DMPC still retained a certain degree of ordering while the HPA3P-bound DMPC became more disordered and the distinctive change in lipid phase transition was absent. This difference may relate to the differences in the helical structure and assembly and orientation of peptides in the DMPC membrane.

Comparison with the effect of peptide binding to DMPC/DMPG indicates that both peptides induced much greater disordering in the mixed DMPC/DMPG bilayer. The birefringence value for DMPC/DMPG dropped to 0.0180 upon binding of HPA3 and to 0.0187 for HPA3P and then further decreased slightly with increases in temperature up to around 25 °C. Above 25 °C, the birefringence values became very similar for both peptides and unlike the peptide-bound DMPC bilayer, the DMPC/DMPG bilayer exhibited no obvious transition over the temperature range with either peptide. Such differences in the phase behaviour between the two bilayers indicate that the final structure of the peptide-bound DMPC/DMPG bilayer is in a much more disordered state than the bilayer alone. In other words, both peptides induce a much greater degree of disorder in a DMPC/DMPG bilayer than in a DMPC bilayer.

4. Discussion

The structural properties and dynamic motion of membranes have been extensively studied with various spectroscopic and diffraction methods [49,54,55]. In spite of the large variation in the lipid compositions found in natural membranes, structural parameters such as lipid packing density, ripple structure, head group packing, thickness and lipid surface area are only available for certain types of lipid molecules [49,54,55]. In terms of peptide–membrane interactions, the inability to fully characterise membrane structure prior to and throughout the peptide binding-dissociation process has limited our complete understanding of the role of membrane structure in the molecular mechanisms of antimicrobial peptide action. The specific interaction of peptides with different lipid components in a

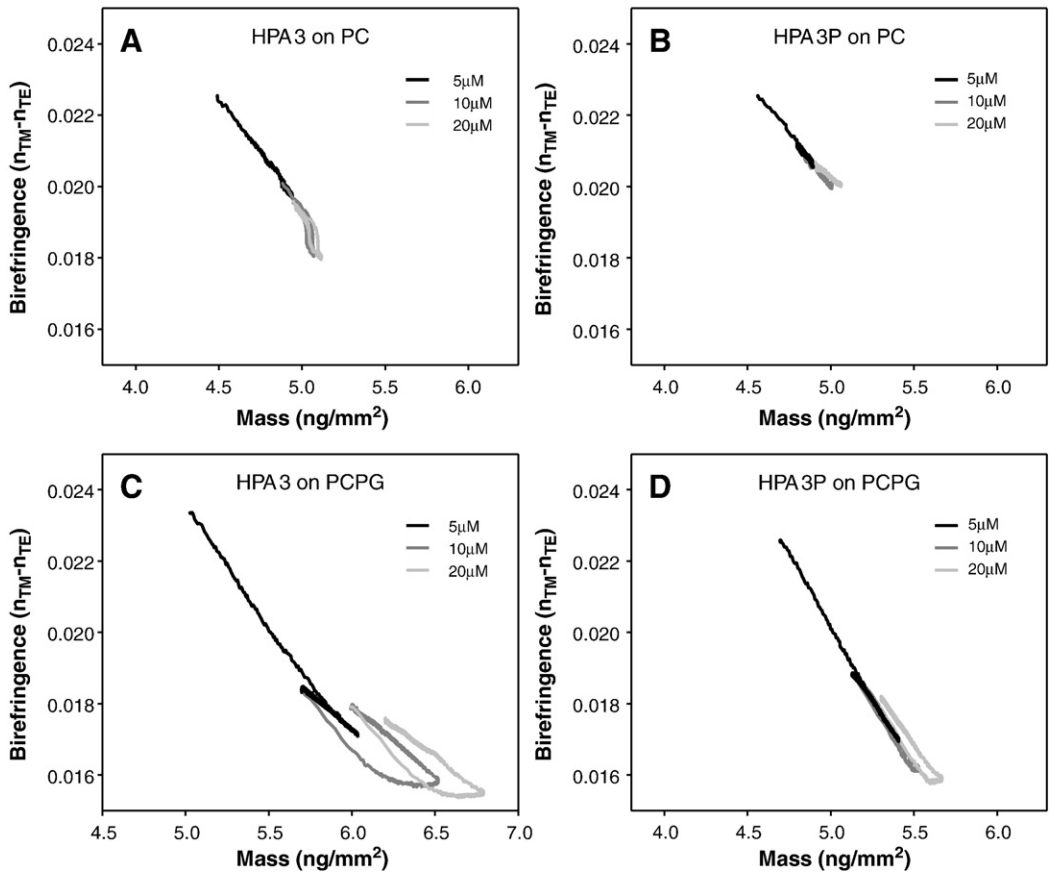

Fig. 7. Hp(2–20) analogues induced changes in membrane lipid order as a function of membrane-bound peptide mass. (A) HPA3 to DMPC, (B) HPA3P to DMPC, (C) HPA3 to DMPC/DMPG and (D) HPA3P to DMPC/DMPG.

membrane causes local perturbations in the structural and dynamic properties of a membrane. The subtle local perturbation in lipid molecules may translate into changes in the global structural properties, such as membrane thinning/thickening and alterations in the acyl chain packing and lipid surface area [56–59]. These changes collectively affect the function of a membrane and subsequent cell activity. The coherent changes in the structure and dynamic motion in peptide and lipid molecules vary in duration and time scale [60]. Hence, greater emphasis is now required to examine the geometrical and dynamic changes that occur within a lipid matrix associated with peptide association–dissociation, insertion, and disruption of membrane integrity. The aim of this study was to document the use of DPI as a biophysical tool that quantifies the effect of peptides on the extent of membrane perturbation through measuring membrane order (birefringence) in real-time as a function of peptide binding.

Hp(2–20) is a peptide derived from the N-terminus of *H. pylori* ribosomal protein L1 and exhibits antimicrobial activity providing a valuable lead candidate as a template for new antibiotics to overcome the threat of drug resistance infection. Among various attempts to enhance or optimise the antimicrobial activity without harming the host cell, one analogue, the HPA3 peptide, with a double substitution of Trp for Gln17 and Asp19, displayed enhanced antibiotic activity without causing haemolysis [24,26]. This enhanced activity was attributed to the increased amphipathicity and overall hydrophobic properties of the linear helical HPA3 peptide. The structure of HPA3 was further modified by the substitution of a proline for a glutamate which induces a bend at the centre of the helix. Previously, the introduction of proline into Hp(2–20) caused a helical break with higher flexibility and significantly reduced the antibiotic activity [61]. Although the preference of these peptides towards negatively charged bacterial membranes has been shown by various cell or lipid vesicle-based assays, little is known about the mechanisms and modes of action employed by these peptides.

Among the wide range of membrane models, DMPC/DMPG [52,62–71] and POPC/POPG [57,64,69,72–75] bilayers are the most commonly used in studies of peptide–membrane interactions. DMPC/DMPG membrane models were chosen in our study for the following reasons: (1) DMPC and DMPG both contain fully saturated acyl chains which allow the effect of disordering by peptides to be minimally affected by the properties of unsaturated double bonds; (2) DMPC and DMPG are extremely well characterised in terms of both physical and structural properties which is important for the validation and confirmation of the high resolution structural data (i.e. thickness $\pm$ 0.1 nm) generated in the DPI experiments; (3) Both DMPC and DMPG have a gel to liquid-crystalline phase transition temperature (Tm) of 23 °C while the Tm for POPC and POPG is −2 °C, a temperature which makes it almost impossible to examine the effect of peptide binding (insertion) on the thermal transition of lipid membranes. These properties offer a significant advantage over POPC/POPG for examining the impact of peptide insertion on the thermal transition of membrane. Moreover, PC-containing phospholipids are the most abundant phospholipid in the eukaryotic membrane and are generally accepted as a good model for the surface membrane of mammalian cells. However, the lipid composition of microbial cells varies from species to species and also changes with growing conditions. Nevertheless, PG-containing lipids are the major lipids in bacterial cell membranes, and particularly in Gram (+) bacteria. The incorporation of DMPG molecules in model DMPC membrane therefore mimics the bacterial cell membrane surface charge. HPA3 and HPA3P are highly positively charged (Table 1) and we therefore

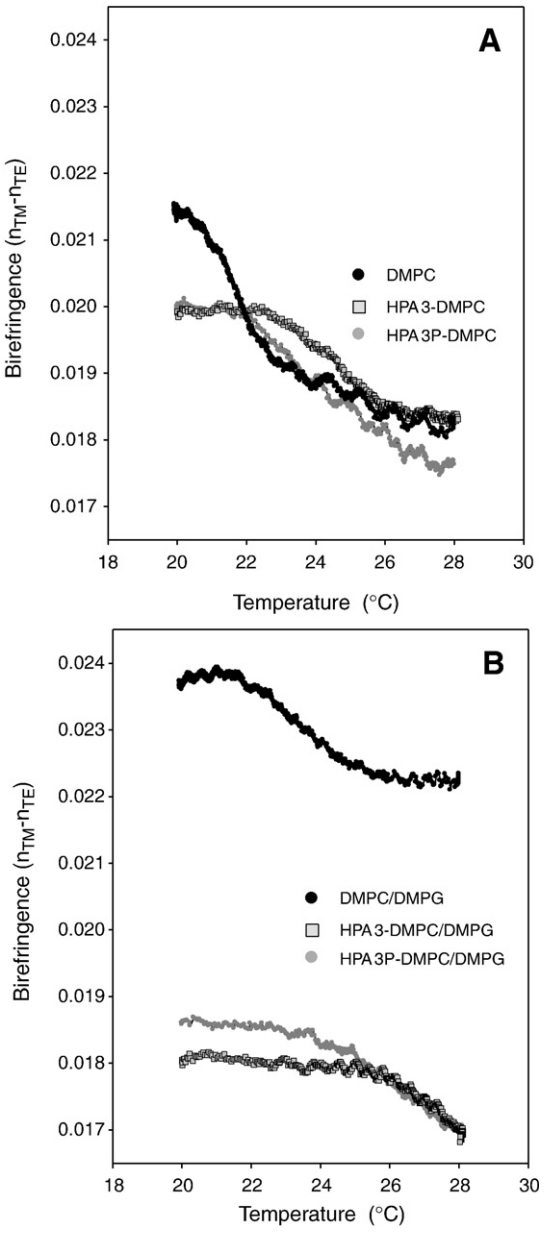

Fig. 8. Effects of Hp(2–20) analogues on the thermal phase transition of adsorbed lipid bilayers. The temperature induced changes to the molecular ordering is used to monitor the phase transition for the same membrane without peptides and post 20 μM peptide binding. (A) Pure DMPC; (B) HPA3 (black) and HPA3P (grey) bound DMPC bilayer; (C) pure DMPC/DMPG (4:1) and (D) HPA3 (black) and HPA3P (grey) bound DMPC/DMPG (4:1) bilayer.

examined the role of electrostatics in modulating peptide structure and binding to these model membranes. The ratio of DMPC to DMPG as 4:1 was chosen as this mixture exhibits the highest phase transition temperature of DMPC/DMPG mixtures [52].

In this study, we quantitatively analysed the membrane binding of these peptides using two optical biosensors to provide information on the relative binding and changes in the membrane structure upon binding. The formation of secondary structure in peptides is a pre-requisite step towards membrane interaction and the degree of secondary structure also impacts on the insertion process. The CD spectra obtained for HPA3 and HPA3P in liposome solution showed that the proline substitution prevented HPA3P from adopting secondary structure in the zwitterionic DMPC membrane and the helical content increased in the presence of negatively charged DMPG molecules. Various studies have shown the important role of electrostatics and bilayer thickness on peptide binding to membranes and these results demonstrate that the negative charge on the membrane surface has a significant effect on the induction of HPA3 and HPA3P helical structure.

The physicochemical properties associated with HPA3 and HPA3P interaction with DMPC and DMPC/DMPG SLBs were quantitatively characterised in terms of their mass bound to different lipid bilayers, extent of changes in membrane molecular ordering as a function of peptide mass and impact on the structural properties of membrane bilayers throughout the entire interaction process. A significant aspect of this study is the ability to fully characterise each single planar bilayer system in terms of a range of dynamic structural parameters including thickness/density, mass, lipid surface area and orientational order. This degree of quantitative characterisation of the bilayer structure enables the real-time action of peptides to be accurately probed in terms of alterations in the dynamic structure of the bilayer. The values for the thickness, mass, density and lipid orientational order of the DMPC membrane prior to peptide binding were smaller than those for the binary DMPC/DMPG membrane. These results when taken together with the smaller area per lipid for DMPC/DMPG (Table 2) indicate a higher packing density for DMPC/DMPG mixed bilayers compared to DMPC membranes, which is consistent with other negatively charged mixed bilayers [52,53]. These results suggest that the DMPC/DMPG bilayer adopts a more ordered alignment of the fatty acyl chains than the pure DMPC bilayer [32].

With respect to the binding of HPA3 to these bilayers, the SPR binding profiles were similar on both DMPC and DMPC/DMPG bilayers in terms of the amount bound and the residual peptide bound after dissociation. However, further probing of this interaction by DPI revealed significant differences in the effect of HPA3 on the two phospholipid bilayers. In particular, the degree of DMPC/DMPG bilayer disruption was double that observed for DMPC upon binding of HPA3. Moreover, the temperature denaturation of DMPC/DMPG was significantly compromised compared to DMPC. These results clearly demonstrate that the presence of negatively charged phospholipids enhances the ability of HPA3 to bind and insert into the membrane and are consistent with data previously obtained from fluorescence quenching studies [25]. Specifically, the less effective quenching of tryptophan fluorescence with anionic lipid vesicles compared to zwitterionic lipid vesicles suggested that HPA3 is buried more extensively in the anionic membrane. In particular, HPA3 has been shown to translocate through the membrane [30,31] and the higher SPR response may reflect a certain degree of translocation which is not possible with the DPI surface.

Comparison of the binding behaviour of HPA3 with HPA3P also revealed significant differences and highlighted the influence of the proline substitution. The SPR profiles revealed a much lower level of binding of HPA3P compared to HPA3. Such large difference in SPR response as a result of introducing proline is not seen between binding to DMPC and DMPC/DMPG. However, while birefringence analysis revealed that HPA3P perturbed the DMPC bilayer less than HPA3, the proline substitution resulted in as large a change in the DMPC/DMPG bilayer structure as HPA3, even though HPA3P bound much less to DMPC/DMPG. These results suggest that the electrostatic interaction between the positively charged face of the peptide and the negatively charged head groups of DMPG facilitates the hydrophobic helix patch insertion into the lipid acyl chain region resulting in greater disordering of the bilayer matrix. HPA3 adopts a linear helical structure while HPA3P is likely to have a kink in the middle of the peptide caused by the proline substitution. The decrease in the helical structure together with the proline-induced kink has clearly exerted a significant influence on the binding mechanism. Firstly, the kink disrupted the hydrophobic membrane binding/insertion face (lower retention time and lower amount bound on both membranes). Secondly, once bound and inserted into

the DMPC/DMPG membrane, HPA3P caused a much higher degree of bilayer disruption per unit peptide mass as it cannot be easily accommodated by the aligned phospholipid chains and cannot translocate through the bilayer.

Overall, these changes in birefringence provide insight into the specific steps associated with the binding of the HPA3 peptides. While it is hard to draw any direct correlations between binding data and cytolytic properties, we can conclude that these peptides have significantly different binding properties and that these differences relate to differences in the effect on membrane structure. Fig. 9 shows a schematic diagram of these steps for both HPA3 and HPA3P. In general, the initial event in peptide–membrane interactions is the association of peptide with a large excess of phospholipid. During this surface interaction, as shown in Fig. 9B, only a small degree of changes in membrane birefringence is measured at low peptide mass. At sufficiently high concentration, the peptides may change their orientation by inserting vertically or at an oblique angle into the lipid bilayer, forming pores of either barrel stave or toroidal type, although the specific angle of the peptide relative to the bilayer normal cannot be determined by DPI (Fig. 9C). After this initial event, the peptide can either dissociate leaving the membrane intact or penetrate the bilayer. A significant degree of membrane perturbation and disruption can then take place and is generally described in terms of a detergent-like carpet mechanism, the induction of non-lamellar lipid phases, or the formation of discrete pores. While the nature of the pore structure cannot be explicitly determined by DPI, peptides undergo significant structural changes upon interaction with membranes which can include oligomerisation. The question of whether a peptide oligomerises within the membrane to form a distinct pore is very difficult to determine and is often assumed to occur based on for example, dye leakage experiments. While oligomerisation can play a significant role for some antimicrobial peptides, and is required to provide a full mechanistic description of peptide disruption, the focus of this paper is the structure of the membrane, irrespective of the oligomerisation state of the peptide. The unique feature of DPI is that it allows us to focus on the bilayer structure and provides a measurement of the membrane birefringence (anisotropy) which is the difference in the refractive index of two different polarised lights (TM and TE). This is a fully quantitative measurement of the lipid packing and ordering of the whole membrane matrix. What the DPI experiments then allow is the direct real-time measurement of the peptide-induced changes to and/or disruption of the bilayer structure which is of primary importance in understanding the molecular mechanisms of antimicrobial peptide action.

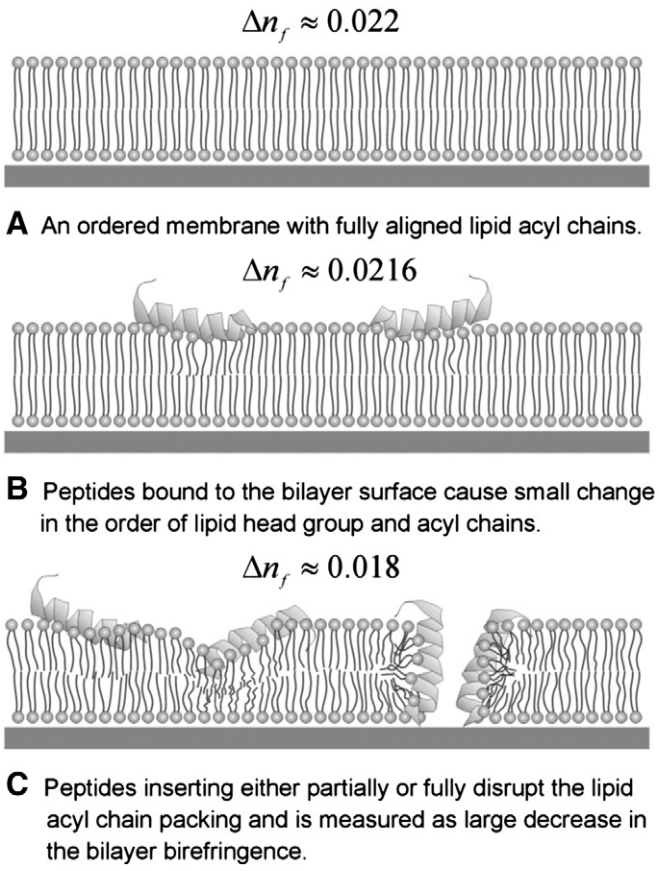

Fig. 9. Schematic of the membrane interaction of the HPA3 peptides depicting the changes in bilayer order as measured by birefringence. (A) An ordered membrane with fully aligned lipid acyl chains where Δn_f is about 0.022; (B) the binding of peptides to the bilayer surface changes the order of the lipid head group resulting in a small decrease in the Δn_f to 0.0216 and (C) the insertion of the peptide partially or fully into the bilayer destroys the lipid acyl chain packing and results in large changes in the degree of ordering resulting in a large decrease in the Δn_f to 0.0180. The birefringence (Δn_f) values obtained for DMPC bilayer at 20 °C were used as examples.

Thus, while it has been shown by leakage and electrophysiology studies [30,31] that the HPA3 peptides form pores, the ability to follow the process by which the pore is formed in terms of changes in bilayer structure allows a significantly more detailed description of HPA3 action. In particular, it is not only the end result of binding/insertion/disruption that is important (i.e. pore or carpet), but also the progressive mechanism by which that final stage is reached that needs to be elucidated. Overall, we have shown that the impact of the Hp(2–20) peptides on membrane structure can be monitored in real-time. However, the action of many cytolytic peptides is associated with loss of material from the support surface including previous studies by our group [65]. While the HPA peptides do not exhibit this behaviour on this system, the results of experiments characterising peptide-induced mass loss and a range of membrane-disruptive behaviour will be reported elsewhere. Nevertheless, the results even with only two peptides demonstrate that the mechanisms of bilayer disturbance differ significantly between two very well characterised phospholipids. Given the enormous range of membrane-active peptides and the associated biological and biophysical properties, the results of our study combined with the results of other biophysical techniques such as fluorescence, Fourier transform infra-red spectroscopy, atomic force microscopy and NMR, will provide a new approach to characterising antimicrobial peptides and will further improve the design and development of effective peptide antibiotics.

Acknowledgements

The financial support of the Faculty of Medicine, Nursing and Health Sciences, Monash University, ATA Scientific, the Australian Research Council and the Potter Foundation is gratefully acknowledged.

References

[1] S.B. Levy, B. Marshall, Antibacterial resistance worldwide: causes, challenges and responses, Nat. Med. 10 (2004) S122–S129.
[2] D.L. Heymann, Resistance to anti-infective drugs and the threat to public health, Cell 124 (2006) 671–675.
[3] G. Taubes, The bacteria fight back, Science 321 (2008) 356–361.
[4] R.E. Hancock, H.G. Sahl, Antimicrobial and host-defense peptides as new anti-infective therapeutic strategies, Nat. Biotechnol. 24 (2006) 1551–1557.
[5] A. Giuliani, G. Pirri, A. Bozzi, A. Di Giulio, M. Aschi, A.C. Rinaldi, Antimicrobial peptides: natural templates for synthetic membrane-active compounds, Cell. Mol. Life Sci. 65 (2008) 2450–2460.
[6] N. Mookherjee, R.E. Hancock, Cationic host defence peptides: innate immune regulatory peptides as a novel approach for treating infections, Cell. Mol. Life Sci. 64 (2007) 922–933.
[7] K.A. Brogden, Antimicrobial peptides: pore formers or metabolic inhibitors in bacteria? Nat. Rev. Microbiol. 3 (2005) 238–250.
[8] M.R. Yeaman, N.Y. Yount, Mechanisms of antimicrobial peptide action and resistance, Pharmacol. Rev. 55 (2003) 27–55.

[9] S.E. Blondelle, K. Lohner, M. Aguilar, Lipid-induced conformation and lipid-binding properties of cytolytic and antimicrobial peptides: determination and biological specificity, Biochim. Biophys. Acta 1462 (1999) 89–108.
[10] R.M. Epand, R.F. Epand, Liposomes as models for antimicrobial peptides, Methods Enzymol. 372 (2003) 124–133.
[11] T.H. Lee, M.I. Aguilar, Trends in the development and application of functional biomembrane surfaces, Biotechnol. Annu. Rev. 12 (2006) 85–136.
[12] K. Lohner, E. Sevcsik, G. Pabst, Liposome-based biomembrane mimetic systems: implications for lipid–peptide interactions, Adv. Planar Lipid Bilayers and Liposomes 6 (2008) 103–137.
[13] K. Lohner, S.E. Blondelle, Molecular mechanisms of membrane perturbation by antimicrobial peptides and the use of biophysical studies in the design of novel peptide antibiotics, Comb. Chem. High Throughput Screen. 8 (2005) 241–256.
[14] I. Wiegand, K. Hilpert, R.E. Hancock, Agar and broth dilution methods to determine the minimal inhibitory concentration (MIC) of antimicrobial substances, Nat. Protoc. 3 (2008) 163–175.
[15] J.D. Hale, R.E. Hancock, Alternative mechanisms of action of cationic antimicrobial peptides on bacteria, Expert Rev. Anti. Infect. Ther. 5 (2007) 951–959.
[16] H.W. Huang, Molecular mechanism of antimicrobial peptides: the origin of cooperativity, Biochim. Biophys. Acta 1758 (2006) 1292–1302.
[17] R.M. Epand, R.F. Epand, Lipid domains in bacterial membranes and the action of antimicrobial agents, Biochim. Biophys. Acta 1788 (2009) 289–294.
[18] M.N. Melo, R. Ferre, M.A. Castanho, Antimicrobial peptides: linking partition, activity and high membrane-bound concentrations, Nat. Rev. Microbiol. 7 (2009) 245–250.
[19] D.G. Lee, Y. Park, H.N. Kim, H.K. Kim, P.I. Kim, B.H. Choi, K.S. Hahm, Antifungal mechanism of an antimicrobial peptide, HP (2–20), derived from N-terminus of *Helicobacter pylori* ribosomal protein L1 against *Candida albicans*, Biochem. Biophys. Res. Commun. 291 (2002) 1006–1013.
[20] K. Putsep, C.I. Branden, H.G. Boman, S. Normark, Antibacterial peptide from *H. pylori*, Nature 398 (1999) 671–672.
[21] K. Putsep, S. Normark, H.G. Boman, The origin of cecropins; implications from synthetic peptides derived from ribosomal protein L1, FEBS Lett. 451 (1999) 249–252.
[22] A. Betten, J. Bylund, T. Christophe, F. Boulay, A. Romero, K. Hellstrand, C. Dahlgren, A proinflammatory peptide from *Helicobacter pylori* activates monocytes to induce lymphocyte dysfunction and apoptosis, J. Clin. Invest. 108 (2001) 1221–1228.
[23] A. de Paulis, N. Prevete, I. Fiorentino, A.F. Walls, M. Curto, A. Petraroli, V. Castaldo, P. Ceppa, R. Fiocca, G. Marone, Basophils infiltrate human gastric mucosa at sites of *Helicobacter pylori* infection, and exhibit chemotaxis in response to *H. pylori*-derived peptide Hp(2–20), J. Immunol. 172 (2004) 7734–7743.
[24] D.G. Lee, H.N. Kim, Y. Park, H.K. Kim, B.H. Choi, C.H. Choi, K.S. Hahm, Design of novel analogue peptides with potent antibiotic activity based on the antimicrobial peptide, HP (2–20), derived from N-terminus of *Helicobacter pylori* ribosomal protein L1, Biochim. Biophys. Acta 1598 (2002) 185–194.
[25] K.H. Lee, D.G. Lee, Y. Park, D.I. Kang, S.Y. Shin, K.S. Hahm, Y. Kim, Interactions between the plasma membrane and the antimicrobial peptide HP (2–20) and its analogues derived from *Helicobacter pylori*, Biochem. J. 394 (2006) 105–114.
[26] S.C. Park, M.H. Kim, M.A. Hossain, S.Y. Shin, Y. Kim, L. Stella, J.D. Wade, Y. Park, K.S. Hahm, Amphipathic alpha-helical peptide, HP (2–20), and its analogues derived from *Helicobacter pylori*: pore formation mechanism in various lipid compositions, Biochim. Biophys. Acta 1778 (2008) 229–241.
[27] Y. Park, S.C. Park, H.K. Park, S.Y. Shin, Y. Kim, K.S. Hahm, Structure–activity relationship of HP (2–20) analog peptide: enhanced antimicrobial activity by N-terminal random coil region deletion, Biopolymers 88 (2007) 199–207.
[28] E.R. Woo, D.G. Lee, Y.S. Chang, Y. Park, K.S. Hahm, Virus-cell fusion inhibitory activity of novel analogue peptides based on the HP (2–20) derived from N-terminus of *Helicobacter pylori* ribosomal protein L1, Protein Pept. Lett. 9 (2002) 477–486.
[29] Y. Park, K.S. Hahm, Effects of N- and C-terminal truncation of HP (2–20) from *Helicobacter pylori* ribosomal protein L1 (RPL1) on its anti-microbial activity, Biotechnol. Lett. 27 (2005) 193–199.
[30] L. Mereuta, T. Luchian, Y. Park, K.S. Hahm, Single-molecule investigation of the interactions between reconstituted planar lipid membranes and an analogue of the HP(2–20) antimicrobial peptide, Biochem. Biophys. Res. Commun. 373 (2008) 467–472.
[31] L. Mereuta, T. Luchian, Y. Park, K.S. Hahm, The role played by lipids unsaturation upon the membrane interaction of the *Helicobacter pylori* HP(2–20) antimicrobial peptide analogue HPA3, J. Bioenerg. Biomembr. 41 (2009) 79–84.
[32] A. Mashaghi, M. Swann, J. Popplewell, M. Textor, E. Reimhult, Optical anisotropy of supported lipid structures probed by waveguide spectroscopy and its application to study of supported lipid bilayer formation kinetics, Anal. Chem. 80 (2008) 3666–3676.
[33] J.F. Popplewell, M.J. Swann, N.J. Freeman, C. McDonnell, R.C. Ford, Quantifying the effects of melittin on liposomes, Biochim. Biophys. Acta 1768 (2007) 13–20.
[34] M.J. Swann, L.L. Peel, S. Carrington, N.J. Freeman, Dual-polarization interferometry: an analytical technique to measure changes in protein structure in real time, to determine the stoichiometry of binding events, and to differentiate between specific and nonspecific interactions, Anal. Biochem. 329 (2004) 190–198.
[35] C.J. Terry, J.F. Popplewell, M.J. Swann, N.J. Freeman, D.G. Fernig, Characterisation of membrane mimetics on a dual polarisation interferometer, Biosens. Bioelectron. 22 (2006) 627–632.
[36] G.H. Cross, A. Reeves, S. Brand, M.J. Swann, L.L. Peel, N.J. Freeman, J.R. Lu, The metrics of surface adsorbed small molecules on the Young's fringe dual slab waveguide interferometer, J. Phys. D 37 (2004).
[37] D. den Engelsen, Optical anisotropy in ordered systems of lipids, Surf. Sci. 56 (1976) 272–280.
[38] K. Mishima, Birefringence studies on effects of additives on bilayer lipid membranes, , 2006.
[39] Z. Salamon, G. Lindblom, G. Tollin, Plasmon-waveguide resonance and impedance spectroscopy studies of the interaction between penetratin and supported lipid bilayer membranes, Biophys. J. 84 (2003) 1796–1807.
[40] Z. Salamon, G. Tollin, Optical anisotropy in lipid bilayer membranes: coupled plasmon-waveguide resonance measurements of molecular orientation, polarizability, and shape, Biophys. J. 80 (2001) 1557–1567.
[41] J.J. Ramsden, Molecular orientation in lipid bilayers, Phil. Mag. B 79 (1999) 381–386.
[42] F.D. Gunstone, J.L. Harwood, Occurrence and characterisation of oils and fats, in: F.D. Gunstone, J.L. Harwood, A.J. Dijkstra (Eds.), The Lipid Handbook, CRC Press, Taylor & Francis Group, Boca Raton, FL, 2007, pp. 37–141.
[43] T.H. Lee, H. Mozsolits, M.I. Aguilar, Measurement of the affinity of melittin for zwitterionic and anionic membranes using immobilized lipid biosensors, J. Pept. Res. 58 (2001) 464–476.
[44] H. Mozsolits, H.J. Wirth, J. Werkmeister, M.I. Aguilar, Analysis of antimicrobial peptide interactions with hybrid bilayer membrane systems using surface plasmon resonance, Biochim. Biophys. Acta 1512 (2001) 64–76.
[45] N. Papo, Y. Shai, Exploring peptide membrane interaction using surface plasmon resonance: differentiation between pore formation versus membrane disruption by lytic peptides, Biochemistry 42 (2003) 458–466.
[46] R. Horvath, J. Ramsden, Quasi-isotropic analysis of anisotropic thin films on optical waveguides, Langmuir 23 (2007) 9330–9334.
[47] S.J. Johnson, T.M. Bayerl, D.C. McDermott, G.W. Adam, A.R. Rennie, R.K. Thomas, E. Sackmann, Structure of an adsorbed dimyristoylphosphatidylcholine bilayer measured with specular reflection of neutrons, Biophys. J. 59 (1991) 289–294.
[48] N. Kucerka, J.F. Nagle, J.N. Sachs, S.E. Feller, J. Pencer, A. Jackson, J. Katsaras, Lipid bilayer structure determined by the simultaneous analysis of neutron and X-ray scattering data, Biophys. J. 95 (2008) 2356–2367.
[49] J.F. Nagle, S. Tristram-Nagle, Structure of lipid bilayers, Biochim. Biophys. Acta 1469 (2000) 159–195.
[50] S. Tristram-Nagle, Y. Liu, J. Legleiter, J.F. Nagle, Structure of gel phase DMPC determined by X-ray diffraction, Biophys. J. 83 (2002) 3324–3335.
[51] L. Yu, L. Guo, J.L. Ding, B. Ho, S.S. Feng, J. Popplewell, M. Swann, T. Wohland, Interaction of an artificial antimicrobial peptide with lipid membranes, Biochim. Biophys. Acta 1788 (2009) 333–344.
[52] R.N. Lewis, Y.P. Zhang, R.N. McElhaney, Calorimetric and spectroscopic studies of the phase behavior and organization of lipid bilayer model membranes composed of binary mixtures of dimyristoylphosphatidylcholine and dimyristoylphosphatidylglycerol, Biochim. Biophys. Acta 1668 (2005) 203–214.
[53] S. Tristram-Nagle, J.F. Nagle, Lipid bilayers: thermodynamics, structure, fluctuations, and interactions, Chem. Phys. Lipids 127 (2004) 3–14.
[54] G. Pabst, Global properties of biomimetic membranes: perspectives on molecular features, Biophys. Rev. Lett. 1 (2006) 57–84.
[55] T. Salditt, Thermal fluctuations and stability of solid-supported lipid membranes, J. Phys. Condens. Matter 17 (2005) R287–R314.
[56] H.W. Huang, F.Y. Chen, M.T. Lee, Molecular mechanism of peptide-induced pores in membranes, Phys. Rev. Lett. 92 (2004) 198304.
[57] C. Li, T. Salditt, Structure of magainin and alamethicin in model membranes studied by X-ray reflectivity, Biophys. J. 91 (2006) 3285–3300.
[58] G. Pabst, S.L. Grage, S. Danner-Pongratz, W. Jing, A.S. Ulrich, A. Watts, K. Lohner, A. Hickel, Membrane thickening by the antimicrobial peptide PGLa, Biophys. J. 95 (2008) 5779–5788.
[59] J. Pan, D.P. Tieleman, J.F. Nagle, N. Kucerka, S. Tristram-Nagle, Alamethicin in lipid bilayers: combined use of X-ray scattering and MD simulations, Biochim. Biophys. Acta 1788 (2009) 1387–1397.
[60] H. Khandelia, J.H. Ipsen, O.G. Mouritsen, The impact of peptides on lipid membranes, Biochim. Biophys. Acta 1778 (2008) 1528–1536.
[61] H. Fu, A. Bjorstad, C. Dahlgren, J. Bylund, A bactericidal cecropin-A peptide with a stabilized alpha-helical structure possess an increased killing capacity but no proinflammatory activity, Inflammation 28 (2004) 337–343.
[62] I.D. Alves, N. Goasdoue, I. Correia, S. Aubry, C. Galanth, S. Sagan, S. Lavielle, G. Chassaing, Membrane interaction and perturbation mechanisms induced by two cationic cell penetrating peptides with distinct charge distribution, Biochim. Biophys. Acta 1780 (2008) 948–959.
[63] E.Y. Chekmenev, B.S. Vollmar, K.T. Forseth, M.N. Manion, S.M. Jones, T.J. Wagner, R.M. Endicott, B.P. Kyriss, L.M. Homem, M. Pate, J. He, J. Raines, P.L. Gor'kov, W.W. Brey, D.J. Mitchell, A.J. Auman, M.J. Ellard-Ivey, J. Blazyk, M. Cotten, Investigating molecular recognition and biological function at interfaces using piscidins, antimicrobial peptides from fish, Biochim. Biophys. Acta 1758 (2006) 1359–1372.
[64] J.T. Cheng, J.D. Hale, M. Elliot, R.E. Hancock, S.K. Straus, Effect of membrane composition on antimicrobial peptides aurein 2.2 and 2.3 from Australian southern bell frogs, Biophys. J. 96 (2009) 552–565.
[65] J.D. Gehman, F. Luc, K. Hall, T.H. Lee, M.P. Boland, T.L. Pukala, J.H. Bowie, M.I. Aguilar, F. Separovic, Effect of antimicrobial peptides from Australian tree frogs on anionic phospholipid membranes, Biochemistry 47 (2008) 8557–8565.
[66] M. Han, Y. Mei, H. Khant, S.J. Ludtke, Characterization of antibiotic peptide pores using cryo-EM and comparison to neutron scattering, Biophys. J. 97 (2009) 164–172.

[67] K.A. Henzler-Wildman, G.V. Martinez, M.F. Brown, A. Ramamoorthy, Perturbation of the hydrophobic core of lipid bilayers by the human antimicrobial peptide LL-37, Biochemistry 43 (2004) 8459–8469.
[68] C. Leidy, L. Linderoth, T.L. Andresen, O.G. Mouritsen, K. Jorgensen, G.H. Peters, Domain-induced activation of human phospholipase A2 type IIA: local versus global lipid composition, Biophys. J. 90 (2006) 3165–3175.
[69] I. Marcotte, K.L. Wegener, Y.H. Lam, B.C. Chia, M.R. de Planque, J.H. Bowie, M. Auger, F. Separovic, Interaction of antimicrobial peptides from Australian amphibians with lipid membranes, Chem. Phys. Lipids 122 (2003) 107–120.
[70] A. Mecke, D.K. Lee, A. Ramamoorthy, B.G. Orr, M.M. Banaszak Holl, Membrane thinning due to antimicrobial peptide binding: an atomic force microscopy study of MSI-78 in lipid bilayers, Biophys. J. 89 (2005) 4043–4050.
[71] G.W. Seto, S. Marwaha, D.M. Kobewka, R.N. Lewis, F. Separovic, R.N. McElhaney, Interactions of the Australian tree frog antimicrobial peptides aurein 1.2, citropin 1.1 and maculatin 1.1 with lipid model membranes: differential scanning calorimetric and Fourier transform infrared spectroscopic studies, Biochim. Biophys. Acta 1768 (2007) 2787–2800.
[72] E.E. Ambroggio, F. Separovic, J.H. Bowie, G.D. Fidelio, L.A. Bagatolli, Direct visualization of membrane leakage induced by the antibiotic peptides: maculatin, citropin, and aurein, Biophys. J. 89 (2005) 1874–1881.
[73] E. Barany-Wallje, S. Keller, S. Serowy, S. Geibel, P. Pohl, M. Bienert, M. Dathe, A critical reassessment of penetratin translocation across lipid membranes, Biophys. J. 89 (2005) 2513–2521.
[74] S.M. Gregory, A. Pokorny, P.F. Almeida, Magainin 2 revisited: a test of the quantitative model for the all-or-none permeabilization of phospholipid vesicles, Biophys. J. 96 (2009) 116–131.
[75] A. Ramamoorthy, S. Thennarasu, D.K. Lee, A. Tan, L. Maloy, Solid-state NMR investigation of the membrane-disrupting mechanism of antimicrobial peptides MSI-78 and MSI-594 derived from magainin 2 and melittin, Biophys. J. 91 (2006) 206–216.